Contribution of canonical nonhomologous end joining to chromosomal rearrangements is enhanced by ATM kinase deficiency

Ragini Bhargava[a,b], Caree R. Carson[a], Gabriella Lee[a], and Jeremy M. Stark[a,b,1]

[a]Department of Cancer Genetics and Epigenetics, Beckman Research Institute of the City of Hope, Duarte, CA 91010; and [b]Irell and Manella Graduate School of Biological Sciences, Beckman Research Institute of the City of Hope, Duarte, CA 91010

Edited by James E. Haber, Brandeis University, Waltham, MA, and approved December 6, 2016 (received for review July 27, 2016)

A likely mechanism of chromosomal rearrangement formation involves joining the ends from two different chromosomal double-strand breaks (DSBs). These events could potentially be mediated by either of two end-joining (EJ) repair pathways [canonical nonhomologous end joining (C-NHEJ) or alternative end joining (ALT-EJ)], which cause distinct rearrangement junction patterns. The relative role of these EJ pathways during rearrangement formation has remained controversial. Along these lines, we have tested whether the DNA damage response mediated by the Ataxia Telangiectasia Mutated (ATM) kinase may affect the relative influence of C-NHEJ vs. ALT-EJ on rearrangement formation. We developed a reporter in mouse cells for a 0.4-Mbp deletion rearrangement that is formed by EJ between two DSBs induced by the Cas9 endonuclease. We found that disruption of the ATM kinase causes an increase in the frequency of the rearrangement as well as a shift toward rearrangement junctions that show hallmarks of C-NHEJ. Furthermore, ATM suppresses rearrangement formation in an experimental condition, in which C-NHEJ is the predominant EJ repair event (i.e., expression of the 3′ exonuclease Trex2). Finally, several C-NHEJ factors are required for the increase in rearrangement frequency caused by inhibition of the ATM kinase. We also examined ATM effectors and found that H2AX shows a similar influence as ATM, whereas the influence of ATM on this rearrangement seems independent of 53BP1. We suggest that the contribution of the C-NHEJ pathway to the formation of a 0.4-Mbp deletion rearrangement is enhanced in ATM-deficient cells.

ATM | C-NHEJ | ALT-EJ | chromosomal rearrangement

Chromosomal deletion rearrangements have been identified in several cancer genome studies. For example, an analysis of cancer cell lines found somatic deletions with an average size of 0.5 Mbp, some of which caused loss of tumor suppressor genes, including *PTEN* and *RB* (1). A likely mechanism for such rearrangements involves aberrant end-joining (EJ) repair that ligates distal ends of two different double-strand breaks (DSBs) on the same chromosome (i.e., distal EJ). Significant insight into deletion rearrangements has been derived from examining V(D)J recombination, which involves EJ repair of programmed DSBs that requires the KU70/KU80 heterodimer that binds DSB ends, DNA ligase 4 (LIG4), and the LIG4 cofactor XRCC4; they are collectively referred to as canonical (classical) nonhomologous end joining (C-NHEJ) (2). Another C-NHEJ factor is XLF, which forms nucleoprotein filaments with XRCC4 to promote LIG4 activity as well as DSB end bridging via an apparent sliding sleeve mechanism (3, 4).

Although C-NHEJ is critical for V(D)J recombination of programmed DSBs, the relative importance of this pathway for other EJ-mediated rearrangements is controversial (5). Namely, another EJ repair pathway, alternative end joining (ALT-EJ), can also contribute to rearrangement formation. ALT-EJ is independent of C-NHEJ factors and mediated by LIG1 and/or LIG3 among other factors (5–7). Repair junctions mediated by these EJ pathways show distinct patterns (6). For example, the repair junctions in C-NHEJ–deficient cells, which by definition, are mediated by ALT-EJ, show a greater frequency of deletion mutations (6). Furthermore, the deletion junctions in C-NHEJ–deficient cells also show frequent microhomology, which refers to short stretches of homology that bridge the DSB ends during EJ (6). Several rearrangement junctions in cancer cells also show evidence of microhomology, which indicates a potential role for ALT-EJ, although microhomology is certainly not required for such rearrangements (8). Accordingly, it is unclear from analysis of such junctions whether ALT-EJ or C-NHEJ is the predominate pathway involved in forming chromosomal rearrangements. As well, the relative role of these EJ pathways could be affected by cellular context, such as the proficiency of DNA damage response (DDR) signaling pathways.

A central DDR pathway is mediated by the Ataxia Telangiectasia Mutated (ATM) kinase, which seems to be important for EJ fidelity, because cells from Ataxia Telangiectasia patients, $Atm^{-/-}$ mice, and cells treated with an inhibitor of ATM kinase activity each show high levels of chromosomal aberrations (9–12). Furthermore, ATM is important to suppress aberrant joining events during both V(D)J recombination and DSB repair in *Saccharomyces cerevisiae* (9, 13). ATM can phosphorylate many targets after DSB induction (11), but one of the central ATM effector pathways involves H2AX (14). In response to DSBs, ATM phosphorylates the histone variant H2AX at S139 (γ-H2AX) (14), which initiates a signaling cascade to recruit several other factors to DSBs, including 53BP1 (15). Given the importance of the ATM-mediated DDR in genome maintenance, we have sought to investigate whether the relative contribution of C-NHEJ vs. ALT-EJ on the formation of chromosomal rearrangements is influenced by this signaling pathway. We developed a reporter system in mouse cells for a 0.4-Mbp deletion

Significance

Chromosomal rearrangements, such as large deletions, can cause loss of tumor suppressor genes. Rearrangements can be formed by aberrant end-joining (EJ) repair that ligates ends from different double-strand breaks. Two distinct EJ pathways could potentially cause rearrangements [canonical nonhomologous end joining (C-NHEJ) and alternative EJ], which are mediated by different factors and cause distinct repair junction patterns. Using a reporter for a 0.4-Mbp deletion rearrangement, we found that cells deficient in the Ataxia Telangiectasia Mutated (ATM) signaling pathway show an increase in the frequency of this rearrangement and a shift toward C-NHEJ–mediated rearrangements. Thus, the relative contribution of distinct EJ pathways to rearrangement formation is affected by ATM signaling, which provides insight into the tumor suppressor function of ATM.

Author contributions: R.B. and J.M.S. designed research; R.B., C.R.C., G.L., and J.M.S. performed research; R.B., C.R.C., G.L., and J.M.S. analyzed data; and R.B. and J.M.S. wrote the paper.

The authors declare no conflict of interest.

This article is a PNAS Direct Submission.

[1]To whom correspondence should be addressed. Email: jstark@coh.org.

This article contains supporting information online at www.pnas.org/lookup/suppl/doi:10.1073/pnas.1612204114/-/DCSupplemental.

rearrangement caused by distal EJ between two DSBs, which are induced by the RNA-guided nuclease Cas9 (16), and have examined the influence of ATM proficiency on the contribution of C-NHEJ to this rearrangement.

Results

The Influence of C-NHEJ Deficiency on a Reporter for a 0.4-Mbp Deletion Rearrangement. We developed an EJ reporter based on green fluorescent protein (EJ6-GFP) (Fig. 1*A* and Fig. S1*A*) to model a large-deletion (0.4-Mbp) rearrangement caused by EJ between distal ends of two tandem DSBs (distal EJ). The reporter consists of a promoterless GFP cassette that is integrated into the *Pim1* gene on chromosome 17 in mouse ES cells (mESCs). The reporter also uses the promoter of the *Cdkn1A* gene, which is 0.4 Mbp upstream of GFP. DSBs are induced in this reporter using Cas9 (16) with two single-guide RNAs (sgRNAs): one targeting exon 1 of the *Cdkn1A* gene (C-sgRNA) and the second targeting a sequence upstream of GFP (G-sgRNA). Distal EJ between these two DSBs causes a 0.4-Mbp deletion rearrangement that places the GFP cassette downstream of the *Cdkn1A* promoter. Thus, coexpression of Cas9 with the C- and G-site sgRNAs in WT mESCs with the EJ6-GFP reporter causes an induction of GFP+ cells, which contain the expected deletion rearrangement (Fig. 1*A* and Fig. S1*B*).

To provide a comparison with distal EJ, we also quantified EJ that uses correct ends flanking a single DSB (i.e., proximal EJ) and that causes mutagenesis at the C site using the surveyor nuclease assay (16, 17) [C-site mutagenesis (C-site mut)] (Fig. 1*A* and Fig. S1*C*). We perform this assay using a portion of each sample, such that the rest of the sample can be used for flow cytometry analysis to determine frequency of GFP+ cells. Subsequently, we calculate the ratio of percentage of GFP+ to percentage of C-site mut (e.g., for a WT sample with 1.06% GFP+ and 8.5% C-site mut, the ratio of percentage of GFP+ to percentage of C-site mut is 12.5×10^{-2}). Quantifying two EJ measurements from the same sample facilitates an internally controlled experiment. Certainly, this analysis does not account for precise EJ, because this EJ event is not distinct from the parental sequence, and it does not address repair by homologous recombination or chromosome loss. An additional limitation of the surveyor assay is that it may underrepresent indel mutation frequencies (*SI Materials and Methods*). Nevertheless, this approach provides the frequency of a 0.4-Mbp deletion rearrangement vs. mutagenic EJ events that do not cause a rearrangement.

To begin to examine the influence of C-NHEJ in this system, we integrated the EJ6-GFP reporter into *Xrcc4*$^{-/-}$ (18) and *Xlf*$^{-/-}$ (19) mESCs, expressed Cas9 and the C- and G-site sgRNAs, and determined the frequency of distal EJ. We found that *Xrcc4*$^{-/-}$, but not *Xlf*$^{-/-}$, showed a modest decrease in distal EJ normalized to C-site mut compared with the WT (Fig. 1*B*). When normalized to transfection efficiency, *Xrcc4*$^{-/-}$ also shows a modest reduction compared with the WT (*P* value above the Bonferroni cutoff), whereas *Xlf*$^{-/-}$ showed a modest increase (Fig. 1*B*). Thus, XRCC4, but not XLF, has a role in promoting distal EJ, albeit in ATM-proficient cells (see below). This distinction between the two factors is consistent with XRCC4 having a greater role than XLF for V(D)J recombination (18, 20). Notably, distal EJ is relatively lower for both *Xrcc4*$^{-/-}$ and *Xlf*$^{-/-}$ when normalized to C-site mut vs. transfection efficiency compared with the WT (Fig. 1*B*). Thus, we considered that both *Xrcc4*$^{-/-}$ and *Xlf*$^{-/-}$ might be prone to elevated mutagenic EJ or conversely, reduced nonmutagenic EJ. A corollary of this hypothesis is that XRCC4 and XLF are required for EJ events that lack insertion or deletion mutations (no indel).

To test this hypothesis, we examined EJ repair junction patterns using amplicon sequencing of the rearrangement (distal EJ) junction from GFP+ sorted cells and found that *Xrcc4*$^{-/-}$ and *Xlf*$^{-/-}$ showed a loss of rearrangement junctions with no indel (Fig. 1*C*). In contrast, such EJ junctions with no indel were readily detectable in the WT (Fig. 1*C*). We also sequenced amplicons of the C site (proximal EJ) from unsorted cells, although quantifying the no indel category in this analysis is not feasible, because such junctions are not distinct from a site that was never cut. In any case, for proximal EJ, we found a significant increase in junctions with >10-nt deletion mutations in *Xrcc4*$^{-/-}$ and *Xlf*$^{-/-}$ compared with the WT (Fig. 1*C*). Furthermore, for both proximal EJ and distal EJ, *Xrcc4*$^{-/-}$ and *Xlf*$^{-/-}$ showed a substantial reduction in deletion mutations without microhomology (0–1 nt) compared with the WT (Fig. 1*C*). Thus, C-NHEJ factors are important for deletion mutations without microhomology and rearrangements without indel mutations and also, suppress proximal EJ junctions with >10-nt deletions. Previous reports have found a similar influence of XRCC4 on repair junctions (6, 21).

C-NHEJ Is the Predominant EJ Repair Event in Cells Expressing the 3′ Exonuclease Trex2. We also developed a distinct experimental condition, in which C-NHEJ is the predominant EJ pathway. Specifically, we tested whether combining expression of Cas9 with the 3′ nonprocessive exonuclease Trex2 might generate DSBs that show a greater reliance on C-NHEJ for EJ repair. Our rationale is that Trex2-mediated degradation of 3′ termini might block ALT-EJ by disrupting the formation of the microhomology-mediated intermediate of this pathway. Furthermore, this approach is based on a prior report showing that coexpression

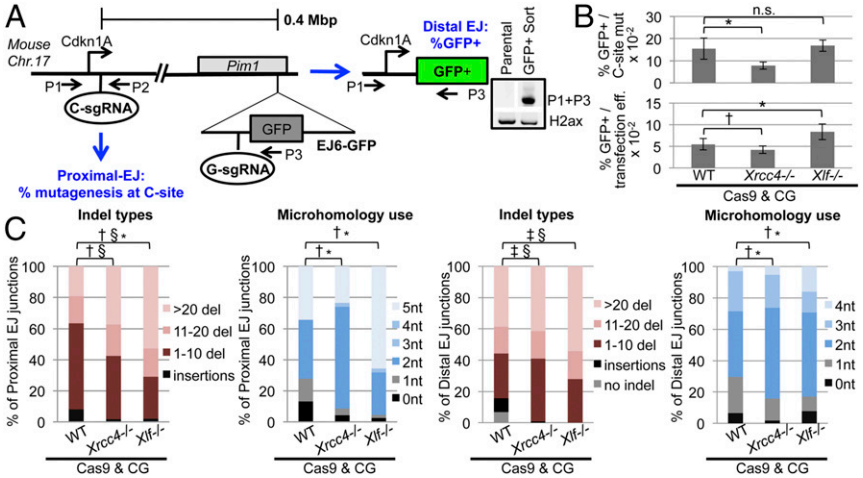

Fig. 1. Examining a 0.4-Mbp deletion rearrangement. (*A*) EJ6-GFP reporter and amplification products for a GFP+ sorted sample. (*B*) Percentage of GFP+ with two different normalizations (C-site mut and transfection efficiency) for transfections of Cas9 and the C- and G-site sgRNAs (Cas9 & CG); $n = 15$ for WT, and $n = 6$ for *Xrcc4*$^{-/-}$ and *Xlf*$^{-/-}$ mESCs. n.s., not significant. *$P < 0.002$; †$P = 0.048$. (*C*) Amplicon deep sequencing analysis of the C site and rearrangements junctions (GFP+ cells) from transfections as in *B* with the percentages of classes of indel mutations (no indel for proximal EJ not included, because this event is not distinct from uncut) as well as microhomology at deletion mutations. Comparisons vs. the WT. For indel types, $P < 0.0001$ and >1.5-fold difference: †>10-nt deletion; ‡no indel; §insertions; *1- to 10-nt deletion. For microhomology use, †$P < 0.0001$ and >1.5-fold difference for no microhomology (0–1 nt), *$P < 0.0001$ for total microhomology patterns.

of I-SceI with Trex2 caused mutagenic proximal EJ events that are dependent on C-NHEJ factors (22).

We examined effects of Trex2 coexpression with Cas9 along with the C- and G-site sgRNAs on EJ repair junctions in WT cells using amplicon deep sequencing (Fig. 2*A* and Figs. S2 and S3). We found that Trex2 expression caused a substantial increase in deletion mutations without microhomology (0–1 nt) for both distal EJ and proximal EJ junctions (Fig. 2*A* and Figs. S2 and S3), which is a hallmark of C-NHEJ. Furthermore, Trex2 expression caused a significant decrease in junctions with large-deletion mutations (>10 nt) for both distal EJ and proximal EJ junctions (Fig. 2*A* and Fig. S3). Thus, Trex2 expression causes a reduction in long-deletion mutations and conversely, an increase in deletion junctions that lack microhomology, thereby causing a shift to junctions with hallmarks of C-NHEJ.

Thus, we hypothesized that C-NHEJ–deficient cells would show defects in EJ repair under conditions of Trex2 expression. We first examined proximal EJ and found that including Trex2 expression abolished detectable levels of C-site mut in both *Xrcc4*$^{-/-}$ and *Xlf*$^{-/-}$ cells (Fig. 2*B*). We then performed complementation analysis using expression vectors for human XRCC4 and mouse XLF along with a mutant of XRCC4 (K169E) that is deficient for DNA binding (3) for an additional negative control. We found that expression of XRCC4 WT (but not K169E) in *Xrcc4*$^{-/-}$ cells and expression of XLF WT in *Xlf*$^{-/-}$ cells each restored detectable C-site mut (Fig. 2*B*). However, using amplicon deep sequencing, we detected indel mutations in a small percentage of products from such samples: 6% for *Xrcc4*$^{-/-}$ and 5% for *Xlf*$^{-/-}$ vs. 18% for the WT (Fig. 2*A*). Notably, because indel mutation frequencies are higher in amplicon sequencing analysis vs. C-site mut (e.g., 18% and 11%, respectively, for the WT), these findings underscore that the surveyor assay may underrepresent indel mutation frequencies. From the sequencing analysis, the *Xrcc4*$^{-/-}$ and *Xlf*$^{-/-}$ samples showed an increase in large-deletion mutations (>10 nt) and a loss of deletion mutations without microhomology (0–1 nt) compared with the WT (Fig. 2*A*). Thus, the small percentage of EJ events in *Xrcc4*$^{-/-}$ and *Xlf*$^{-/-}$ cells with a mutation at the C site showed a pattern consistent with ALT-EJ. Because mutagenic EJ is reduced in *Xrcc4*$^{-/-}$ and *Xlf*$^{-/-}$ cells with Trex2 expression, the remainder of DSBs is likely repaired by homologous recombination as described previously (23) or may remain unrepaired.

We next examined distal EJ (i.e., percentage of GFP+ cells) in these experiments. Because proximal EJ causing C-site mut was undetectable in both *Xrcc4*$^{-/-}$ and *Xlf*$^{-/-}$ mESCs (Fig. 2*B*), we relied on another approach for normalization of distal EJ (i.e., transfection efficiency) and performed complementation analysis. We found that expression of XRCC4 WT (but not K169E) in *Xrcc4*$^{-/-}$ and expression of XLF WT in *Xlf*$^{-/-}$ cells each caused an increase in the frequency of distal EJ (Fig. 2*C*). These findings indicate that, under conditions of Trex2 expression, C-NHEJ is important for both proximal EJ causing C-site mut and distal EJ. Thus, we suggest that including Trex2 expression provides an approach to examine EJ that is predominantly mediated by C-NHEJ.

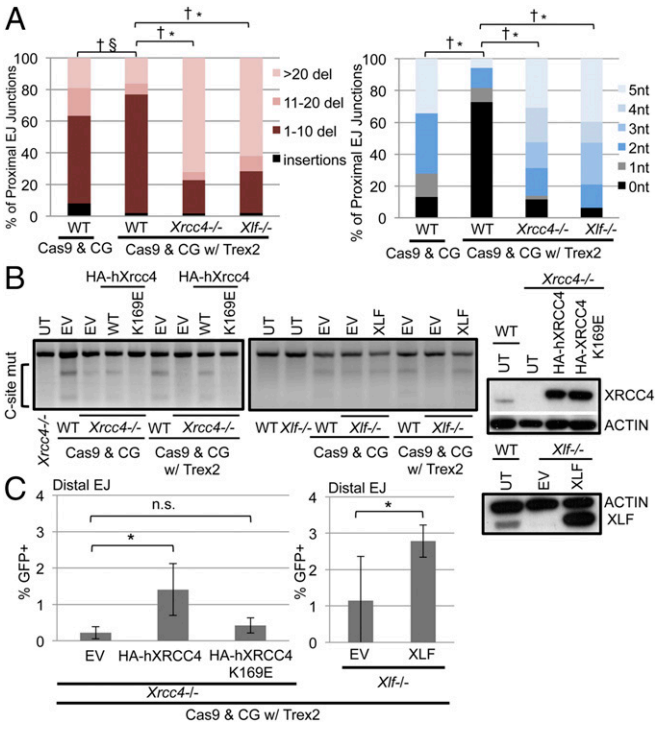

Fig. 2. Cells expressing the 3′ nonprocessive exonuclease Trex2 show an enhanced requirement for C-NHEJ for EJ repair. (*A*) Shown is deep sequencing analysis of amplicons of the C site performed as in Fig. 1*C*. The WT junctions without Trex2 are the same as in Fig. 1*C*. Comparisons vs. the WT. (*Left*) $P <$ 0.0001 and >1.5-fold difference: †>10-nt deletion; §insertions; *1- to 10-nt deletion. (*Right*) †$P < 0.0001$ and >1.5-fold difference for no microhomology (0–1 nt), *$P < 0.0001$ for total microhomology patterns. (*B*) Shown are products of the surveyor nuclease assay to measure C-site mut from representative transfections. Also shown are immunoblots confirming expression of XRCC4 and XLF. EV, control empty vector. (*C*) Shown is the percentage of GFP+ (distal EJ) for transfections as in *B*, each normalized to transfection efficiency. Cas9 & CG, Cas9 and the C- and G-site sgRNAs; n.s., not significant; UT, untransfected. *$P < 0.003$ ($n = 6$ for *Xrcc4*$^{-/-}$ and $n = 12$ for *Xlf*$^{-/-}$).

The Role of C-NHEJ on Deletion Rearrangement Formation Is Enhanced in ATM-Deficient Cells. We then sought to test the hypothesis that deletion rearrangements formed in ATM-deficient cells are primarily mediated by C-NHEJ. We performed the EJ6-GFP reporter assay without Trex2 expression in *Atm*$^{-/-}$ mESCs (24) and found that these cells showed an increase in distal EJ compared with WT mESCs (Fig. 3*A* and Fig. S4*A*) (*P* value normalized to transfection efficiency above the Bonferroni cutoff). Furthermore, the fold increase in distal EJ for *Atm*$^{-/-}$ cells was more pronounced when normalized to C-site mut vs. transfection efficiency, indicating that ATM deficiency may cause an increase in EJ events with no indel mutations (Fig. 3*A* and Fig. S4*A*). Thus, we examined rearrangement junction patterns and found that *Atm*$^{-/-}$ cells showed a marked increase in rearrangement junctions with no indel mutations (Fig. 3*B*). Furthermore, these rearrangement junctions showed a decrease in large-deletion mutations (>10 nt) and an increase the frequency of deletion mutations without microhomology (0–1 nt) (Fig. 3*B*). Similar findings were observed for WT cells treated with an Ataxia Telangiectasia Mutated kinase inhibitor (ATMi) (Fig. 3 *A* and *B*) (12). Notably, transfections in this entire study without ATMi were treated with vehicle control (DMSO) to facilitate direct comparisons. These findings indicate that ATM deficiency causes an increase in deletion rearrangement frequency as well as a marked shift toward rearrangement junctions that show hallmarks of C-NHEJ.

Because the rearrangement junctions in ATM-deficient cells are consistent with a greater reliance on C-NHEJ, we next tested whether the elevated rearrangement frequency in ATM-deficient cells would persist under conditions that require C-NHEJ for EJ repair (i.e., experiments with Trex2). From these experiments, we found that *Atm*$^{-/-}$ cells showed a marked increase in distal EJ compared with WT mESCs (Fig. 3*C* and Fig. S4*A*). We also analyzed rearrangement junctions in *Atm*$^{-/-}$ mESCs from transfections with Trex2 and found that the junction pattern is consistent with a substantial contribution of C-NHEJ, such as for WT mESCs (Fig. 3*D*). Similar results were observed with WT cells treated with ATMi (Fig. 3 *C* and *D*) and U2OS human cells treated with ATMi using a previously described reporter for distal EJ between two DSBs that causes a short-deletion rearrangement (EJ5-GFP) (Fig. S4*B*) (25). Thus, ATM deficiency causes a marked increase in deletion

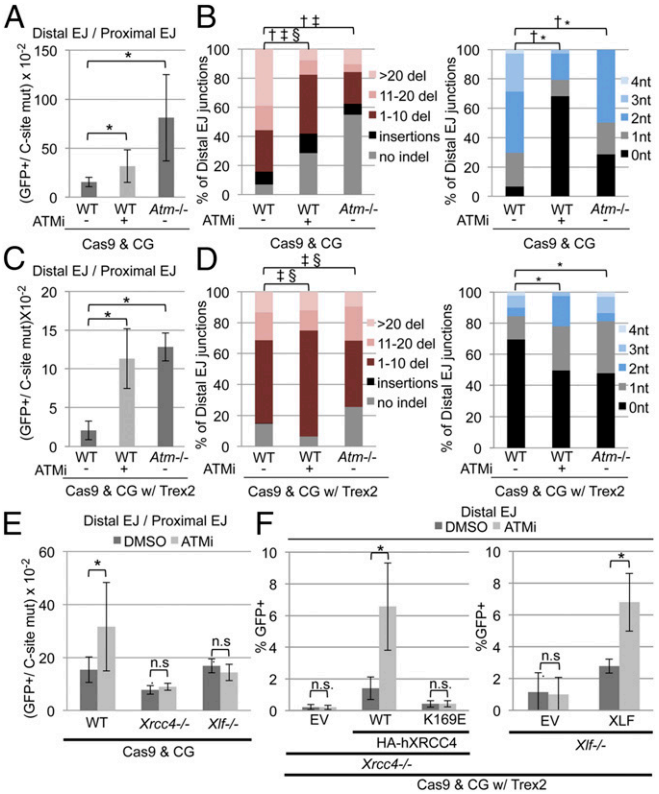

Fig. 3. The influence of C-NHEJ on a 0.4-Mbp deletion rearrangement is markedly enhanced by ATM deficiency. (*A*) Shown is the ratio of percentage of GFP+ to percentage of C-site mut for transfections with Cas9 and the C- and G-site sgRNAs (Cas9 & CG). WT cells were also treated with ATMi. All transfections without ATMi were treated with vehicle control (DMSO). The transfections for the WT without ATMi are the same as in Fig. 1*B*. *$P \leq 0.0014$ ($n \geq 12$ for the WT and $n = 5$ for $Atm^{-/-}$ mESCs). (*B*) Shown are rearrangement junctions from GFP+ sorted cells from transfections as in *A*. Distal EJ junctions for the WT (no ATMi) are the same as in Fig. 1*C*. Comparisons vs. the WT. (*Left*) $P <$ 0.0001 and >1.5-fold difference: †>10-nt deletion; ‡no indel; §insertions. (*Right*) †$P < 0.0001$ and >1.5-fold difference for no microhomology (0–1 nt), *$P <$ 0.0001 for total microhomology patterns. (*C*) Repair frequencies are shown as in *A* for transfections including Trex2. *$P < 0.0001$ ($n = 15$ for WT, and $n = 6$ for $Atm^{-/-}$ mESCs). (*D*) Shown are rearrangement junctions from transfections with Trex2, which were analyzed as in *B*. (*E*) For the transfections without Trex2, shown are repair values as in *A*. *$P = 0.0014$ ($n \geq 12$ for the WT, and $n = 6$ for $Xrcc4^{-/-}$ and $Xlf^{-/-}$ mESCs). (*F*) For the transfections with Trex2, complementation vectors were included, and shown is the percentage of GFP+ (distal EJ) normalized to transfection efficiency. The values for the transfections without ATMi are the same as in Fig. 2*C*. EV, control empty vector; n.s., not significant. *$P \leq 0.0013$ ($n = 6$ for $Xrcc4^{-/-}$, and $n = 12$ for $Xlf^{-/-}$ mESCs).

rearrangements under conditions in which C-NHEJ is the predominant EJ pathway.

We then tested the converse of this finding, namely whether effects of ATM deficiency on rearrangement formation require C-NHEJ. Specifically, we examined the effect of ATMi treatment on the frequency of distal EJ in $Xrcc4^{-/-}$ and $Xlf^{-/-}$ mESCs. Beginning with experiments without Trex2, we found that ATMi treatment showed no effect on distal EJ in either $Xrcc4^{-/-}$ or $Xlf^{-/-}$ mESCs, whereas such treatment in WT cells caused a twofold increase (Fig. 3*E*). Similarly, in experiments that included Trex2, we found that ATMi treatment showed no effect on distal EJ in either $Xrcc4^{-/-}$ or $Xlf^{-/-}$ mESCs (Fig. 3*F*). Importantly, complementation with XRCC4 and XLF using transient expression in the respective cell lines restored the increase in distal EJ caused by ATMi treatment both with and without Trex2 expression (Fig. 3*F* and Fig. S4*C*). We also examined another C-NHEJ factor in this system, Ku70, using $Ku70^{-/-}$ mESCs (26) and found similar results as with XRCC4 and XLF (Fig. S5). These findings indicate that several C-NHEJ factors (XRCC4, XLF, and KU70) are required for ATMi treatment to cause an increase in distal EJ. Accordingly, the relative role of C-NHEJ on the formation of a 0.4-Mbp deletion rearrangement is enhanced by ATM deficiency.

Influence of ATM Effectors H2AX and 53BP1 on Deletion Rearrangements. We then examined two effector proteins that are integral to the ATM-mediated DDR: H2AX and 53BP1. Using $H2ax^{-/-}$ mESCs (27) with the EJ6-GFP reporter without Trex2 expression, we found that $H2ax^{-/-}$ cells showed an increase in distal EJ, which was unaffected by ATMi treatment (Fig. 4*A* and Fig. S4*A*) (*P* value normalized to transfection efficiency above the Bonferroni cutoff). As with $Atm^{-/-}$ cells, this increase in distal EJ was more pronounced when normalized to C-site mut, indicating that H2AX loss might also cause an increase in EJ with no indel mutations. Therefore, we examined the effect of H2AX loss on distal EJ junctions and found a similar shift as caused by ATM deficiency: an increase in rearrangements without an indel mutation, an increase in deletion mutations without microhomology, and a decrease in >10-nt deletion mutations (Fig. 4*B*). These data indicate that H2AX loss causes an increase in the frequency of a 0.4-Mbp deletion rearrangement and a shift in junction patterns consistent with C-NHEJ, which are similar to the effects of ATM deficiency. We then performed experiments with Trex2 expression and found a significant increase in distal EJ in $H2ax^{-/-}$ cells relative to WT cells (Fig. 4*A* and Fig. S4*A*). Also, transient expression of H2AX WT but not a mutant of the ATM phosphorylation site (S139A) (14) in $H2ax^{-/-}$ cells inhibited distal EJ in experiments with Trex2 (Fig. S6*A*). ATMi treatment also caused an additional increase in distal EJ in $H2ax^{-/-}$ cells with Trex2 expression, but the fold effect is substantially lower than for the WT (Fig. 4*A*) (2.7- vs. 5.4-fold, respectively; $P < 0.002$). Finally, the junction patterns from experiments with Trex2 were not substantially affected by H2AX loss compared with the WT (Fig. 4*B*). These findings indicate that H2AX functions in the same pathway as ATM to suppress a 0.4-Mbp deletion rearrangement caused by C-NHEJ, although ATM shows an additional H2AX-independent role in this process.

We also examined 53BP1 by generating $53bp1^{-/-}$ mESCs by targeting Cas9 upstream of its essential Tudor domain (Fig. S6*B*) (28). Using the EJ6-GFP reporter without Trex2 expression, $53bp1^{-/-}$ showed a modest increase in distal EJ compared with the WT (Fig. 4*C* and Fig. S4*A*) (significant increase normalized to C-site mut but not significantly different normalized to transfection efficiency). Importantly, ATMi treatment of $53bp1^{-/-}$ caused a significant increase in distal EJ that was similar to the effect of ATMi on the WT (Fig. 4*C*). Analogous results were found using the Trex2 approach (Fig. 4*C* and Fig. S4*A*). We also examined the distal EJ junctions in $53bp1^{-/-}$ and found a distinct pattern: the frequency of rearrangements with no indel mutations was increased compared with the WT, whereas the frequency of deletion mutations without microhomology (0–1 nt) was markedly reduced (Fig. 4*B*). In contrast, $53bp1^{-/-}$ cells treated with ATMi showed a similar junction pattern as WT cells treated with ATMi (Figs. 3*B* and 4*B*). We also generated and tested a $53bp1^{-/-}Xlf^{-/-}$ EJ6-GFP reporter line (Fig. S6*B*). We found that XLF expression had no effect on distal EJ in the $53bp1^{-/-}Xlf^{-/-}$ mESCs (Fig. 4*D*). In contrast, for $53bp1^{-/-}Xlf^{-/-}$ mESCs treated with ATMi, XLF expression caused a substantial increase in distal EJ (Fig. 4*D*), such as for $Xlf^{-/-}$ cells (Fig. S4*C*). These results indicate that the influence of XLF on distal EJ is similar between $53bp1^{-/-}$ and WT cells. Thus, loss of 53BP1 does not cause an obvious increase in the relative role of C-NHEJ in rearrangement formation. In summary, these results indicate that the influence of ATM on the formation of a 0.4-Mbp deletion rearrangement is independent of 53BP1. Finally, we examined two small molecule inhibitors and found that a DNA-dependent protein kinase (DNA-PKcs)

GENETICS

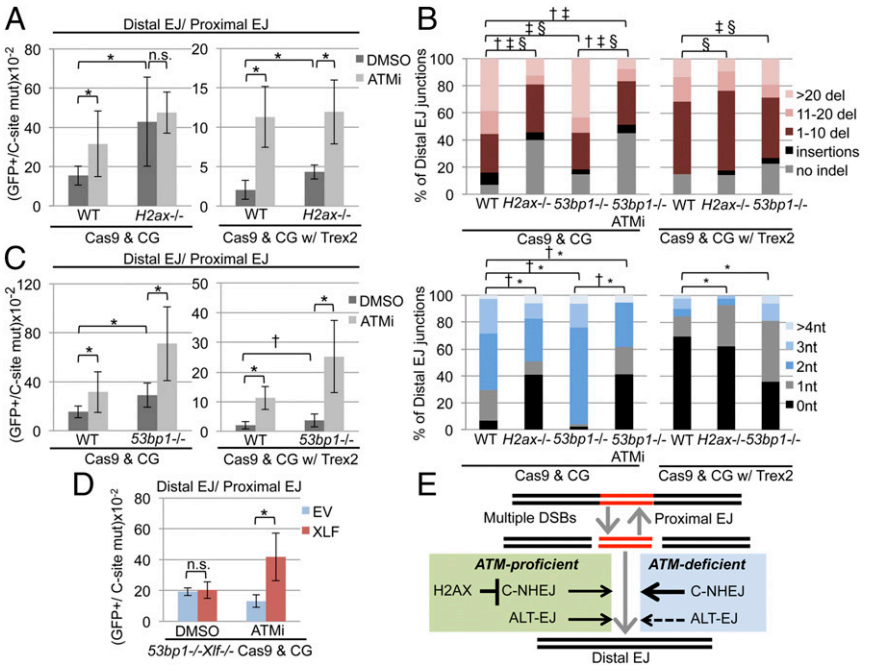

Fig. 4. Influence of the ATM effectors H2AX and 53BP1 on a 0.4-Mbp deletion rearrangement. (*A*) Shown are repair frequencies for transfections of *H2ax*$^{-/-}$ cells with the EJ6-GFP reporter as in Fig. 3 *A* and *C*. The WT frequencies are the same as in Fig. 3 *A* and *C*. *$P \leq 0.0014$ ($n \geq 5$ for *H2ax*$^{-/-}$, and $n \geq 12$ for WT mESCs). n.s., not significant. (*B*) Shown are rearrangement junctions for *H2ax*$^{-/-}$ and *53bp1*$^{-/-}$ mESCs examined as in Fig. 1*C*. WT junctions are the same as Figs. 1*C* and 3 *B* and *D*. Comparisons vs. WT or no ATMi. (*Top*) $P < 0.0001$ and >1.5-fold difference: †>10-nt deletion; ‡no indel; §insertions. (*Bottom*) †$P < 0.0001$ and >1.5-fold difference for no microhomology (0–1 nt), *$P < 0.0001$ for total microhomology patterns. (*C*) Shown are repair frequencies for transfections of *53bp1*$^{-/-}$ cells with the EJ6-GFP reporter as in Fig. 3 *A* and *C*. The WT transfections are the same as in Fig. 3 *A* and *C*. *$P \leq 0.0014$; †$P = 0.021$ ($n = 12$ for *53bp1*$^{-/-}$, and $n \geq 12$ for the WT). (*D*) Shown are repair frequencies for transfections of *53bp1*$^{-/-}$*Xlf*$^{-/-}$ mESCs with the EJ6-GFP reporter with Cas9 and the C- and G-site sgRNAs (Cas9 & CG) along with either control EV or XLF expression vector and treated with either ATMi or DMSO. *$P = 0.0078$ ($n = 6$). (*E*) Shown is a model for the influence of ATM on the relative role of C-NHEJ in chromosomal rearrangement formation.

inhibitor (NU7441) caused a modest increase in distal EJ normalized to C-site mut, whereas a poly ADP-ribose polymerase inhibitor (olaparib, which we confirmed inhibits ALT-EJ) did not cause substantial effects on distal EJ (Fig. S7).

Discussion

Defining the pathways that contribute to chromosomal rearrangement formation is important to understand the etiology of cancer and the cellular response to clastogenic cancer therapeutics. Rearrangement junctions from cancer cells show patterns consistent with a mixture of ALT-EJ and C-NHEJ, such that the relative contribution of these pathways to rearrangement formation has been unclear (5). Using an assay for a large-deletion (0.4-Mbp) rearrangement, we have presented evidence that disruption of the ATM-mediated DDR causes an increase in the relative contribution of the C-NHEJ pathway to this rearrangement. Thus, although C-NHEJ is important for genome stability, this pathway may nevertheless facilitate cancer-associated rearrangements, particularly in cells with a defective ATM-mediated DDR. Consistent with this notion, inherited and somatic mutations in *ATM* have been associated with several types of cancer (29).

The role of C-NHEJ on chromosomal rearrangement formation has been controversial. XRCC4 was shown to promote a 3.2-kb deletion rearrangement between two I-SceI–induced DSBs in hamster cells (6). Similarly, XRCC4 and LIG4 have been shown to promote chromosomal rearrangements in human cells, specifically short intrachromosomal deletions and translocations that are induced by two DSBs using pairs of TALEN or Cas9 nucleases (21). However, the findings of these studies contradict a report in mouse cells showing that XRCC4 suppresses the formation of chromosomal translocations induced by I-SceI (30). Accordingly, the role of C-NHEJ in chromosomal rearrangements has been proposed to be species-specific (21). Although the role of C-NHEJ in chromosomal rearrangement formation may show some species-specific differences for individual rearrangement types, our findings indicate that the proficiency of the ATM-mediated DDR of a particular cell type can significantly influence the relative role of XRCC4 and other C-NHEJ factors on rearrangement formation.

Another implication of our findings is that the ATM-mediated DDR seems to regulate C-NHEJ to limit aberrant EJ events. Namely, ATM loss causes not only a shift toward junction patterns consistent with C-NHEJ but also, an increase in the frequency of C-NHEJ events that cause rearrangements. Indeed, under experimental conditions where C-NHEJ is the predominant repair event (i.e., Trex2 expression), we find that ATM deficiency causes a substantial increase in the frequency of distal EJ. ATM could suppress aberrant C-NHEJ events by several mechanisms, including ensuring that DSB ends are properly paired before assembly of the complete functional C-NHEJ complex. We suggest that defining the phosphorylation targets of ATM important for suppressing aberrant C-NHEJ will be important for understanding the etiology of chromosomal rearrangements.

Along these lines, we examined two central ATM targets, H2AX and 53BP1. We found that *H2ax*$^{-/-}$ cells showed a very similar EJ phenotype as ATM-deficient cells: an elevated frequency of distal EJ and a shift in the rearrangement junction pattern toward C-NHEJ. H2AX also appears to function in the same pathway as ATM, because the fold effect of ATMi treatment on distal EJ was diminished in *H2ax*$^{-/-}$ cells. Furthermore, an H2AX mutant with loss of the ATM phosphorylation site (S139A) failed to suppress distal EJ. Consistent with an elevated role for C-NHEJ in H2AX-deficient cells, *H2ax*$^{-/-}$*Xlf*$^{-/-}$ mice have been shown to be embryonic lethal, whereas the single mutants are

viable (20). Furthermore, *H2ax*$^{-/-}$ mice show elevated chromosomal translocations caused by V(D)J recombination (31), similar to ATM-deficient mice (9, 11). Our findings may seem inconsistent with a report showing elevated end degradation of V(D)J recombination intermediates in *H2ax*$^{-/-}$ cells; however, the repair of these DSBs requires nuclease cleavage to open the hairpin coding ends (32), which are distinct from Cas9-induced DSBs. Although the precise role of H2AX in limiting aberrant C-NHEJ is unclear, γ-H2AX can spread for several kilobases from DSBs (33) and thereby, mediate an expansive DDR signal that could contribute to the regulation of C-NHEJ.

We also found that 53BP1 has a distinct influence on rearrangement formation compared with ATM. For one, we observed an increase in microhomology use at the junctions in *53bp1*$^{-/-}$ cells, which may represent elevated ALT-EJ. Furthermore, ATMi treatment had a similar effect on *53bp1*$^{-/-}$ cells as on the WT, and the influence of XLF on distal EJ was not affected by loss of 53BP1. These findings indicate that the influence of ATM on suppressing deletion rearrangements is independent of 53BP1. Although the deletion rearrangement modeled in our study does not require 53BP1, this factor has been shown to be important for other types of chromosomal rearrangements: fusion of dysfunctional telomeres and class switch recombination (28). However, the chromosomal contexts of these rearrangements are distinct. Namely, dysfunctional telomeres are one-sided DSBs and hence, lack an appropriately paired DSB end for proximal EJ that could compete with the telomere fusion event. As well, the rearrangements caused by class switch recombination seem to involve a higher-order chromosome structure to favor the rearrangement (34). In conclusion, we suggest that the relative influence of C-NHEJ on chromosomal rearrangement formation is magnified in cells deficient in ATM and H2AX but not 53BP1.

Materials and Methods

Cell Lines and Plasmids. The WT mESC line was from ATCC (J1). The *Xrcc4*$^{-/-}$, *Xlf*$^{-/-}$, *H2ax*$^{-/-}$, *Ku70*$^{-/-}$, and *Atm*$^{-/-}$ mESCs were previously described (18, 19, 24, 26, 27). The *53bp1*$^{-/-}$ and *53bp1*$^{-/-}$ *Xlf*$^{-/-}$ mESC lines were generated using Cas9-mediated gene editing (Fig. S6*B*). The pimEJ6-GFP reporter was derived from pimEJ5-GFP and used for *Pim1* targeting of the mESC lines (7). The sgRNA/Cas9 plasmids were derived from px330 (16) (Addgene 42230 deposited by Feng Zhang) (sgRNA sequences in Fig. S1*A*). The pCAGGS-BSKX (EV), pCAGGS-Trex2, pCAGGS-KU70, and pCAGGS-XRCC4 plasmids were previously described (7, 23), and the latter used to add an HA tag and generate the K169E mutant. The pCAGGS-Xlf plasmid was derived from the Mammalian Gene Collection clone 8243.

DSB Reporter Assays. mESCs ($0.5–2 \times 10^5$) were plated on a 12-well plate and subsequently transfected with 1.2 μg total plasmid (each in equal amounts) using 3.6 μL Lipofectamine 2000 (Invitrogen/Thermofisher) in 1 mL antibiotic-free media. Transfection media were removed after 4 h and replaced with media containing either ATMi (12) (10 μM KU55933; EMD Millipore 118500 or Selleckchem S1092) or vehicle (DMSO). Three days post-transfection, a portion of the sample was used to determine GFP+ frequencies by flow cytometry. With the rest of the sample, genomic DNA was purified for quantifying mutation of the C-sgRNA site using the Surveyor Mutation Detection Kit (IDT#706020) (*SI Materials and Methods*). Repair frequencies normalized to transfection efficiency used parallel transfections with pCAGGS-NZE-GFP. Similar transfections were used for immunoblotting analysis (*SI Materials and Methods*). Each repair value is the mean of at least three independent transfections, error bars reflect the SD, and statistics were performed with the unpaired *t* test with Bonferroni correction. Amplicon deep sequencing analysis was performed using the Illumina HiSeq2500 platform (*SI Materials and Methods*).

ACKNOWLEDGMENTS. Drs. Xiwei Wu, Jinhui Wang, and Sean Howard provided assistance. This work was supported by National Cancer Institute of the NIH Grants R01CA120954 (to J.M.S.), R01CA197506 (to J.M.S.), and P30CA33572 (for City of Hope Core Facilities).

1. Bignell GR, et al. (2010) Signatures of mutation and selection in the cancer genome. *Nature* 463(7283):893–898.
2. Alt FW, Zhang Y, Meng FL, Guo C, Schwer B (2013) Mechanisms of programmed DNA lesions and genomic instability in the immune system. *Cell* 152(3):417–429.
3. Andres SN, et al. (2012) A human XRCC4-XLF complex bridges DNA. *Nucleic Acids Res* 40(4):1868–1878.
4. Brouwer I, et al. (2016) Sliding sleeves of XRCC4-XLF bridge DNA and connect fragments of broken DNA. *Nature* 535(7613):566–569.
5. Pannunzio NR, Li S, Watanabe G, Lieber MR (2014) Non-homologous end joining often uses microhomology: Implications for alternative end joining. *DNA Repair (Amst)* 17:74–80.
6. Guirouilh-Barbat J, Rass E, Plo I, Bertrand P, Lopez BS (2007) Defects in XRCC4 and KU80 differentially affect the joining of distal nonhomologous ends. *Proc Natl Acad Sci USA* 104(52):20902–20907.
7. Howard SM, Yanez DA, Stark JM (2015) DNA damage response factors from diverse pathways, including DNA crosslink repair, mediate alternative end joining. *PLoS Genet* 11(1):e1004943.
8. Stephens PJ, et al. (2009) Complex landscapes of somatic rearrangement in human breast cancer genomes. *Nature* 462(7276):1005–1010.
9. Callén E, et al. (2007) ATM prevents the persistence and propagation of chromosome breaks in lymphocytes. *Cell* 130(1):63–75.
10. White JS, Choi S, Bakkenist CJ (2008) Irreversible chromosome damage accumulates rapidly in the absence of ATM kinase activity. *Cell Cycle* 7(9):1277–1284.
11. Shiloh Y, Ziv Y (2013) The ATM protein kinase: Regulating the cellular response to genotoxic stress, and more. *Nat Rev Mol Cell Biol* 14(4):197–210.
12. Hickson I, et al. (2004) Identification and characterization of a novel and specific inhibitor of the ataxia-telangiectasia mutated kinase ATM. *Cancer Res* 64(24): 9152–9159.
13. Lee K, Zhang Y, Lee SE (2008) Saccharomyces cerevisiae ATM orthologue suppresses break-induced chromosome translocations. *Nature* 454(7203):543–546.
14. Burma S, Chen BP, Murphy M, Kurimasa A, Chen DJ (2001) ATM phosphorylates histone H2AX in response to DNA double-strand breaks. *J Biol Chem* 276(45): 42462–42467.
15. Celeste A, et al. (2002) Genomic instability in mice lacking histone H2AX. *Science* 296(5569):922–927.
16. Ran FA, et al. (2013) Genome engineering using the CRISPR-Cas9 system. *Nat Protoc* 8(11):2281–2308.
17. Guschin DY, et al. (2010) A rapid and general assay for monitoring endogenous gene modification. *Methods Mol Biol* 649:247–256.
18. Gao Y, et al. (1998) A critical role for DNA end-joining proteins in both lymphogenesis and neurogenesis. *Cell* 95(7):891–902.
19. Zha S, Alt FW, Cheng HL, Brush JW, Li G (2007) Defective DNA repair and increased genomic instability in Cernunnos-XLF-deficient murine ES cells. *Proc Natl Acad Sci USA* 104(11):4518–4523.
20. Zha S, et al. (2011) ATM damage response and XLF repair factor are functionally redundant in joining DNA breaks. *Nature* 469(7329):250–254.
21. Ghezraoui H, et al. (2014) Chromosomal translocations in human cells are generated by canonical nonhomologous end-joining. *Mol Cell* 55(6):829–842.
22. Bennardo N, Stark JM (2010) ATM limits incorrect end utilization during non-homologous end joining of multiple chromosome breaks. *PLoS Genet* 6(11):e1001194.
23. Bennardo N, Gunn A, Cheng A, Hasty P, Stark JM (2009) Limiting the persistence of a chromosome break diminishes its mutagenic potential. *PLoS Genet* 5(10):e1000683.
24. Xu Y, Baltimore D (1996) Dual roles of ATM in the cellular response to radiation and in cell growth control. *Genes Dev* 10(19):2401–2410.
25. Gunn A, Stark JM (2012) I-SceI-based assays to examine distinct repair outcomes of mammalian chromosomal double strand breaks. *Methods Mol Biol* 920:379–391.
26. Gu Y, Jin S, Gao Y, Weaver DT, Alt FW (1997) Ku70-deficient embryonic stem cells have increased ionizing radiosensitivity, defective DNA end-binding activity, and inability to support V(D)J recombination. *Proc Natl Acad Sci USA* 94(15):8076–8081.
27. Bassing CH, et al. (2002) Increased ionizing radiation sensitivity and genomic instability in the absence of histone H2AX. *Proc Natl Acad Sci USA* 99(12):8173–8178.
28. Lottersberger F, Bothmer A, Robbiani DF, Nussenzweig MC, de Lange T (2013) Role of 53BP1 oligomerization in regulating double-strand break repair. *Proc Natl Acad Sci USA* 110(6):2146–2151.
29. Choi M, Kipps T, Kurzrock R (2016) ATM mutations in cancer: Therapeutic implications. *Mol Cancer Ther* 15(8):1781–1791.
30. Simsek D, Jasin M (2010) Alternative end-joining is suppressed by the canonical NHEJ component Xrcc4-ligase IV during chromosomal translocation formation. *Nat Struct Mol Biol* 17(4):410–416.
31. Yin B, et al. (2009) Histone H2AX stabilizes broken DNA strands to suppress chromosome breaks and translocations during V(D)J recombination. *J Exp Med* 206(12): 2625–2639.
32. Helmink BA, et al. (2011) H2AX prevents CtIP-mediated DNA end resection and aberrant repair in G1-phase lymphocytes. *Nature* 469(7329):245–249.
33. Iacovoni JS, et al. (2010) High-resolution profiling of gammaH2AX around DNA double strand breaks in the mammalian genome. *EMBO J* 29(8):1446–1457.
34. Dong J, et al. (2015) Orientation-specific joining of AID-initiated DNA breaks promotes antibody class switching. *Nature* 525(7567):134–139.